

THE OFFICIAL MAGAZINE OF THE OCEANOGRAPHY SOCIETY

Oceanography

CITATION

Farmer, D.M., M.H. Alford, R.-C. Lien, Y.J. Yang, M.-H. Chang, and Q. Li. 2011. From Luzon Strait to Dongsha Plateau: Stages in the life of an internal wave. *Oceanography* 24(4):64–77, <http://dx.doi.org/10.5670/oceanog.2011.95>.

DOI

<http://dx.doi.org/10.5670/oceanog.2011.95>

COPYRIGHT

This article has been published in *Oceanography*, Volume 24, Number 4, a quarterly journal of The Oceanography Society. Copyright 2011 by The Oceanography Society. All rights reserved.

USAGE

Permission is granted to copy this article for use in teaching and research. Republication, systematic reproduction, or collective redistribution of any portion of this article by photocopy machine, reposting, or other means is permitted only with the approval of The Oceanography Society. Send all correspondence to: info@tos.org or The Oceanography Society, PO Box 1931, Rockville, MD 20849-1931, USA.

From Luzon Strait to Dongsha Plateau Stages in the Life of an Internal Wave

BY DAVID M. FARMER, MATTHEW H. ALFORD, REN-CHIEH LIEN,
YIING JIANG YANG, MING-HUEI CHANG, AND QIANG LI

A rainbow and tropical clouds over the aft deck of R/V *Revelle* during the 2010 IWISE (Internal Waves in Straits Experiment) pilot cruise. The yellow steel sphere in the foreground provided flotation for one of the moorings discussed in the text.

ABSTRACT. Tidal currents in Luzon Strait south of Taiwan generate some of the largest internal waves anywhere in the ocean. Recent collaborative efforts between oceanographers from the United States and Taiwan explored the generation, evolution, and characteristics of these waves from their formation in the strait to their scattering and dissipation on Dongsha Plateau and the continental slope of mainland China. Nonlinear internal waves affect offshore engineering, navigation, biological productivity, and sediment resuspension. Observations within Luzon Strait identified exceptionally large vertical excursions of density (as expressed primarily in temperature profiles) and intense turbulence as tidal currents interact with submarine ridges. In the northern part of the strait, the ridge spacing is close to the internal semidiurnal tidal wavelength, allowing wave generation at both ridges to contribute to amplification of the internal tide. Westward radiation of semidiurnal internal tidal energy is predominant in the north, diurnal energy in the south. The competing effects of nonlinearity, which tends to steepen the stratification, and rotational dispersion, which tends to disperse energy into inertial waves, transform waves traveling across the deep basin of the South China Sea. Rotation inhibits steepening, especially for the internal diurnal tide, but despite the rotational effect, the semidiurnal tide steepens sufficiently so that nonhydrostatic effects become important, leading to the formation of a nonlinear internal wave train. As the waves encounter the continental slope and Dongsha Plateau, they slow down, steepen further, and are modified and scattered into extended wave trains. At this stage, the waves can “break,” forming trapped cores. They have the potential to trap prey, which may account for their attraction to pilot whales, which are often seen following the waves as they advance toward the coast. Interesting problems remain to be explored and are the subjects of continuing investigations.

INTRODUCTION

With the increasing extent and quality of remotely sensed images of the ocean, the widespread occurrence of patterns caused by nonlinear internal waves (also called internal solitary waves) in coastal waters becomes ever more apparent. The nonlinearity in this case is expressed in the progressive distortion of the shape of the internal tide, with consequent steepening of density surfaces to the point where nonhydrostatic dispersion, associated with vertical acceleration of the fluid, becomes important, and short-period waves are formed. Once formed, these waves approximate a balance between the nonlinearity, which tends to concentrate the energy, and dispersion,

which tends to spread it out, so that the waves retain their distinctive shape as they travel (see also Box 1). Individual waves can exist in isolation, and thus are described as internal solitary waves, internal solitons, or just “solitons.” They form some of the most striking features of the ocean surface, modulating surface roughness to produce great arcs that, in extreme cases, can stretch hundreds of kilometers while typically retaining a width of ~ 5 km or less. The waters around Taiwan generate prominent examples of these waves. Their importance to navigation, offshore engineering, underwater acoustical propagation, and sediment suspension, as well as the mixing, stirring, and aggregation of

prey that can impact the biological environment, have motivated intense study. Moreover, their inherent nonlinearity presents a fascinating scientific challenge to those seeking to explain and predict their properties and behavior.

Although various mechanisms can generate nonlinear internal waves, the primary source is typically strong tidal currents leading to dynamic interaction between stratified water and topographic features, such as submarine ridges and the continental slope. They are, therefore, most common near abrupt or irregular topography in coastal waters. The internal waves generated just south of Taiwan in Luzon Strait are among the largest observed anywhere in the ocean and can often be tracked by remote sensing as they cross the deep basin of the South China Sea. The remotely sensed patterns are associated with short-period nonlinear internal waves. These waves do not form in the deep basin on all tides, but invariably occur as the internal tide starts to interact with the continental shelf of mainland China where they slow down, can form trapped cores, and scatter and decay. A collaboration of many scientists supported by the Physical Oceanography Program of the US Office of Naval Research, together with prominent scientific and logistical backing from Taiwan, is currently focusing efforts on understanding the origin, evolution, physical behavior, and biological effects of these waves. Here, we provide an overview of some of the results and draw attention to outstanding features that await further investigation. Our focus is on recent measurements in Luzon Strait (an energetic source of internal tides; Alford et al., 2011), observations, and simplified analysis of the

BOX 1. NONLINEAR FLUID DYNAMICAL BEHAVIOR

Nonlinearity in this article refers to nonlinear fluid dynamical behavior. Nonlinear terms are present in the equations of motion of fluid dynamics. For example, terms may be of the form “velocity, or vertical displacement of a density interface, multiplied by a gradient of the same property.” Although these terms are always present, for some problems they can be neglected. However, they can also be important, even dominant, in certain situations, and this is true for internal waves that are steep; for a given wave length, nonlinearity increases with amplitude. Nonlinear waves exhibit many characteristics that distinguish them from the linear wave approximation. For example, the slope of the wave can change with time (i.e., gets steeper or less steep depending on whether the slope is positive or negative and depending on water depth and density stratification). One consequence of this behavior is that an initially sinusoidal wave can evolve into a sawtooth wave. When the wave becomes sufficiently steep, vertical acceleration becomes important, and the resulting vertical motions lead to the formation of higher-frequency waves (a process referred to as nonhydrostatic dispersion). Thus, a consequence of nonlinearity is that the shape of the internal tide can change as the interface between less-dense water near the surface and denser water at depth becomes distorted, eventually forming internal waves that exhibit a much shorter period than that of the internal tide from which they evolved. Thus, the nonlinearity, combined with nonhydrostatic dispersion, creates the short-period waves we see in the deep basin of the South China Sea.

That's one part of the wave evolution problem. Another part is that Earth's rotation disperses energy from the steepening internal tide into motions initially transverse to the wave propagation (rotational dispersion) to form “inertial waves.” There is a competition between the nonlinearity that steepens the internal tide and the rotation that extracts energy from the internal tide. The rotational dispersion is greater for the diurnal tide because its period (24 h) is closer to the inertial period (33 h) than is true for the semidiurnal tide.

waves' transformation as they propagate westward, including formation of short-period nonlinear internal waves in the deep basin (Li and Farmer, 2011), their interaction with the shoaling seafloor and with Dongsha Island (Lien, 2005), and evidence of biological interactions. While the generation, propagation, and fate of the waves has attracted much study in recent years, our selective focus on these features provides three diverse views of the waves from their origin in Luzon Strait to their interaction with the Dongsha Plateau.

TIDAL INTERACTION AND TURBULENCE IN LUZON STRAIT

The internal waves radiating westward across the deep basin of the northern South China Sea have their origin in Luzon Strait, south of Taiwan. Surprisingly, there is little evidence in remotely sensed images, either in the Pacific to the east or within Luzon Strait itself, of the narrow elongated surface features so clearly seen in remotely sensed images of the deep basin further west (Figure 1). The sharp western boundary of the northward-flowing Kuroshio is a prominent feature of the strait that occasionally intrudes in a great loop into the South China Sea, but more often skirts Luzon Strait between the two submarine ridges (Rudnick et al., 2011, in this issue). The Kuroshio, although likely influencing their generation, changes its shape on a scale of weeks to months and is unlikely to be the direct source of the waves we observe. In contrast, the barotropic tidal currents, primarily running east-west, force the thermally stratified waters of the strait across a complex topography characterized by two ridges, Heng-Chun to the west and Lan-Yu to the east. The

western ridge is shallower to the north, and the eastern ridge is shallower to the south and punctuated by islands; the two ridges are closer to each other in the south. It is one of the intriguing consequences of nonlinear evolution of the internal tides that the highly irregular and complex topography of Luzon Strait can lead to the smoothly shaped coherent features characteristic of remotely sensed images in the far field.

A major challenge to those seeking to model the generation and evolution of these internal waves is the wide range of scales involved. The topography of Luzon Strait is rugged and complex, and the depth of the South China Sea varies from ~ 4,000 m in the deep basin to 100–300 m on the Dongsha Plateau and the continental shelf of mainland China. Moreover, nonlinearity transforms the internal tides with scales of 100–200 km into trains of large-amplitude, steep internal waves. A comprehensive model must be three dimensional and nonhydrostatic, with sufficient resolution to handle the nonlinear transformation. Zhang et al. (2011) show that such modeling is now becoming possible. Their model results lead to some important insights, confirming, for example, that the primary internal tide generation

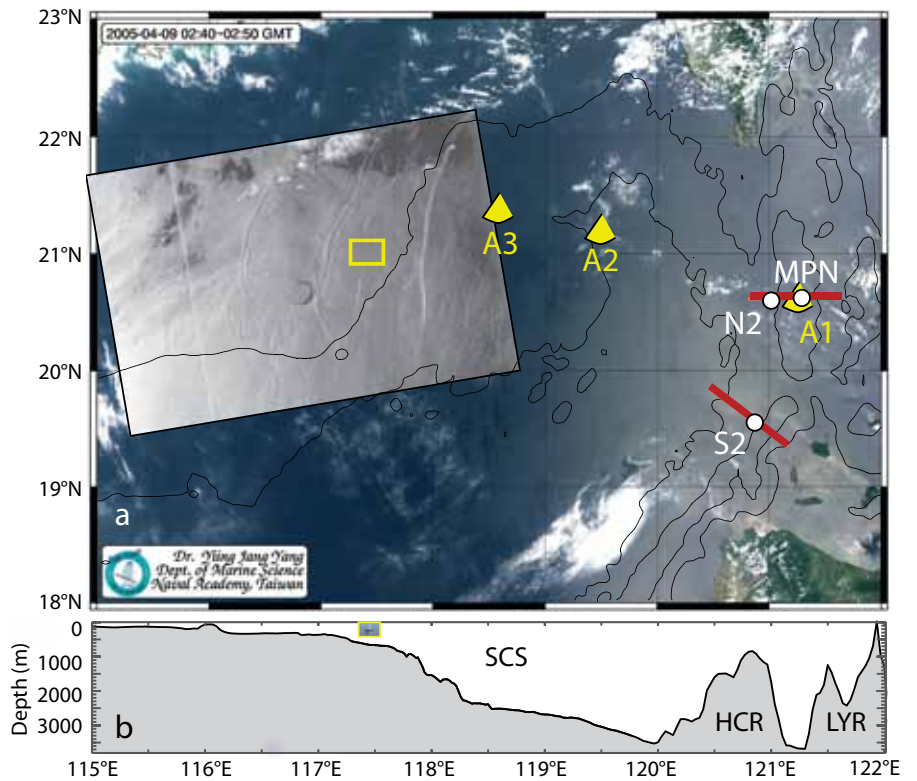


Figure 1. (a) Chart of South China Sea superimposed on a MODIS remotely sensed image illustrating the surface signature of nonlinear internal waves and measurement locations. Red lines: 2010 observations of Luzon Strait. A1, A2, and A3 show 2007 PIES (pressure-sensor equipped inverted echosounders) deployments. Yellow rectangle: ship-based observations of shoaling internal waves. (b) Bathymetry along 21°N. SCS = South China Sea. HCR = Heng-Chun Ridge. LYR = Lan-Yu Ridge.

occurs over the eastern ridge and that the variable ridge orientation from north to south preferentially radiates waves in different directions into the South China Sea. They distinguish between the generation of so-called A-waves

(which occur as nonlinear internal wave packets in the deep basin) and B-waves (which initially evolve as single large-amplitude waves), and show that A-waves are preferentially radiated from the southern part of Luzon Strait, where diurnal internal tidal beams augment the semidiurnal wave, and propagate into the northern portion of the South China Sea basin, whereas B-waves, which are reinforced by the ridge spacing and slopes, are preferentially radiated into the southern portion. Reconciliation of such comprehensive model calculations with the finely resolved measurements in Luzon Strait discussed below—as well as more recent observations—remains a task for the future. However, given the hydrodynamics of a complex

David M. Farmer (dfarmer@gso.uri.edu) is Professor Emeritus, The Graduate School of Oceanography, University of Rhode Island, Narragansett, RI, USA. **Matthew H. Alford** is Senior Oceanographer and Associate Professor, Applied Physics Laboratory, University of Washington, Seattle, WA, USA. **Ren-Chieh Lien** is Principal Oceanographer and Affiliate Professor, Applied Physics Laboratory, University of Washington, Seattle, WA, USA. **Yiing Jiang Yang** is Associate Professor, Department of Marine Science, Naval Academy, Tsoying, Kaohsiung, Taiwan. **Ming-Huei Chang** is Assistant Professor, Department of Marine Environmental Informatics, National Taiwan Ocean University, Keelung, Taiwan. **Qiang Li** was a PhD candidate at the Graduate School of Oceanography, University of Rhode Island, Narragansett, RI, USA, and is currently Assistant Professor, Center for Ocean Science and Technology, Graduate School at Shenzhen, Tsinghua University, Shenzhen, China.

environment such as the South China Sea, simplified models can also prove helpful, and in a subsequent section we include results from a simplified two-layer model that help explain some of the observed features.

A diverse array of measurements

these inversions is related to the outer scale of turbulence. By sorting them as described by Thorpe (1977), it is possible to estimate the turbulent kinetic energy dissipation rate. This approach provides results consistent with direct microstructure measurements (Dillon, 1982;

shows an example at two sample stations (N2 and S6) on the eastern flank of the western ridge with velocity, represented by color (left two panels) and dissipation rate (right panel). Each station was occupied twice: once at a time of predominantly semidiurnal forcing (first and third rows) and once when diurnal signals were dominant (second and fourth rows). Density contours in each panel show the vertical displacement of isopycnals, which can reach 500 m close to the steep face of the western ridge at the northern station. The measurements are generally consistent with the expected ebb and flood of the tides, with large turbulence dissipations observed each 12 and 24 hours, respectively. Superimposed on these energetic tidal currents, the northward flow of the Kuroshio appears as a red patch in the upper 500 m, especially noticeable during both occupations of the northern station.

“ WITH THE INCREASING EXTENT AND QUALITY OF REMOTELY SENSED IMAGES OF THE OCEAN, THE WIDESPREAD OCCURRENCE OF PATTERNS CAUSED BY NONLINEAR INTERNAL WAVES (ALSO CALLED INTERNAL SOLITARY WAVES) IN COASTAL WATERS BECOMES EVER MORE APPARENT. ”

acquired in a short but intensive observational program during the summer of 2010 have already revealed important features of tidal interaction with the topography in Luzon Strait (Alford et al., 2011). The goal was to acquire preliminary observations of the internal tide in the strait so as to estimate energy and energy fluxes of the semidiurnal and diurnal components, as well as the rate of turbulent kinetic energy dissipation. Observations were made along two lines shown in Figure 1 and included repeated conductivity-temperature-depth (CTD) and acoustic Doppler current profiler (ADCP) measurements that yielded profiles of temperature, salinity, density, and current velocity over almost the entire water column at approximately hourly intervals.

Numerous inversions in the measured density profiles are interpreted as regions where turbulence has swept dense water upward, and the vertical scale of

Alford et al., 2006) and is especially appropriate for rapid estimates over the full water column in this intensely turbulent environment. (Although these comparisons were carried out for smaller overturns than presented here [overturns occur when dense water moves up and over less-dense water, a process that takes energy and leads to some degree of mixing], the relationships appear to hold for these large overturns, as indicated by preliminary comparisons with simultaneous temperature microstructure measurements. Detailed comparisons are the topic of ongoing work.)

Repeated profiling at each location for 36 hours can reliably separate semidiurnal and diurnal signals. These measurements are important in Luzon Strait, where both semidiurnal and diurnal tides are significant and the timing of astronomical forcing leads to periods where one or the other tide is dominant (see Figures 2 and 4). Figure 2

As expected for this region of intense tidal interaction with topography, the magnitude of the baroclinic velocity is $\sim 1 \text{ m s}^{-1}$ peak-to-peak, the vertical displacement of isopycnals in the weakly stratified water below 1,000 m is 200–500 m, and dissipation rates are up to $10^{-5} \text{ W kg}^{-1}$, much stronger than open-ocean conditions. Dissipation rates are greatest at N2 and are some of the largest observed, implying vertical diffusivity exceeding $10^{-1} \text{ m}^2 \text{ s}^{-1}$, over 10,000 times that of typical open ocean values (Gregg, 1989) and a thousand times that of Munk's (1966) 1D global estimate.

The spatial pattern of dissipation can be seen from profiles along the northern and southern lines (Figure 3). Left and right panels refer to semidiurnal and diurnal energy and energy flux signals (light and dark gray, respectively),

discussed below. Each panel shows profiles of the logarithm of total dissipation rate (not separated by frequency) with a yellow/green color map. Dissipation increases toward the bottom at all stations, where the internal tide and topography can be expected to interact most strongly. In spite of observational limitations, the northern ridge appears more dissipative.

Preliminary two-dimensional numerical simulations (Maarten

Buijsman, Geophysical Fluid Dynamics Laboratory, Princeton University, *pers. comm.*, 2011) match the magnitude and phase of the observed velocity, isopycnal displacement, and dissipation signals quite well at some locations such as N2, pointing to the role of internal hydraulic processes and wave breaking on the steep western ridge. Ridge separation in northern Luzon Strait is comparable to the semidiurnal internal tide wavelength. Echeverri and Peacock (2010), and

Buijsman et al. (2010a) have explored the resonance that can occur in such environments. Resonance encompasses a broad range of processes, but for our purposes here, we loosely define it as wave generation between the two ridges leading to reinforcement of the signal.

Returning to Figure 3, the potential for resonance of the northern and southern lines is seen by overplotting internal-wave characteristics (lines with slopes corresponding to the angle

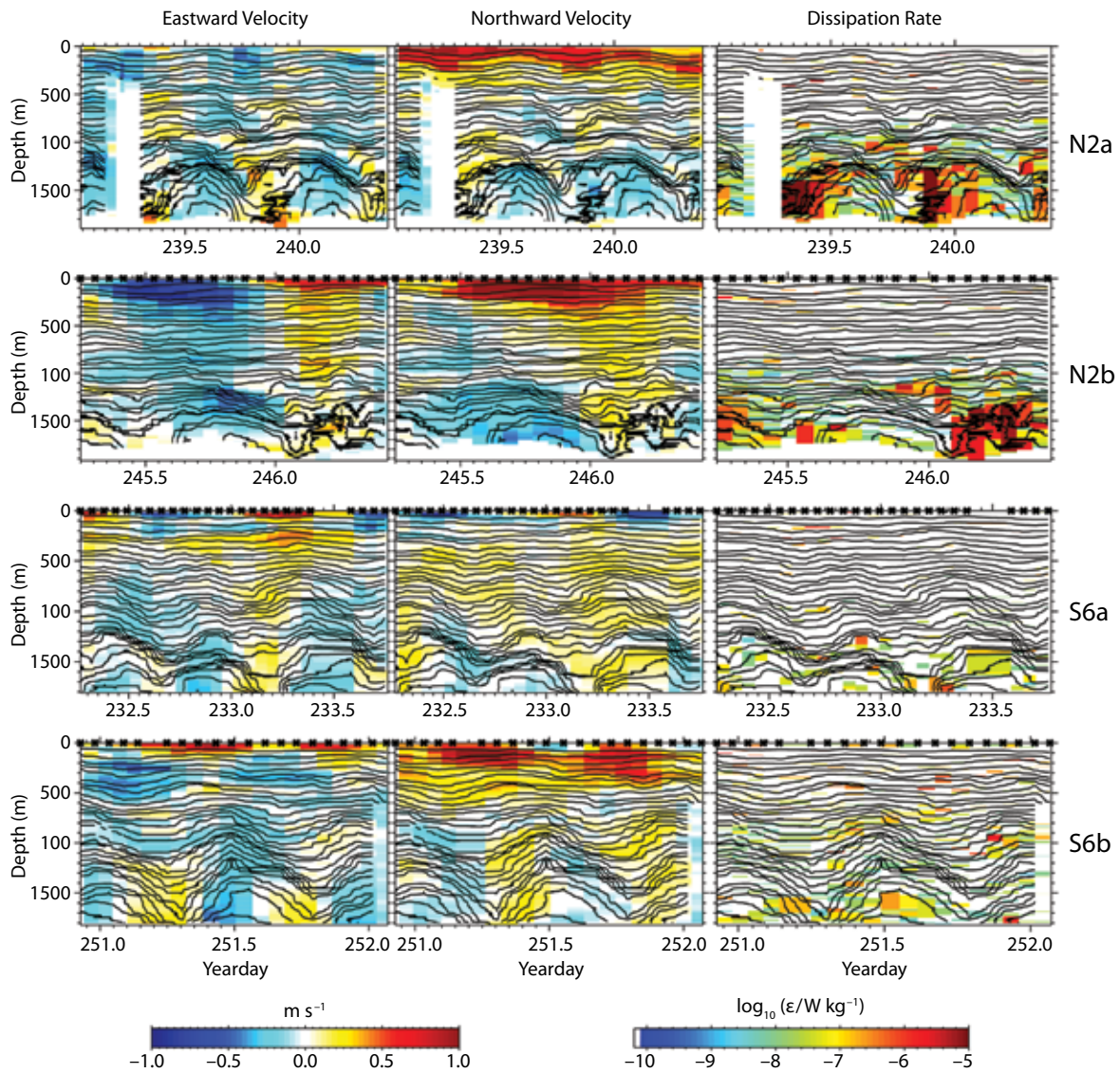


Figure 2. Top row: Time series of eastward (left) and northward (middle) velocity, and Thorpe-inferred turbulent dissipation rate (right) for station N2a. The superimposed density contours (black lines) are evenly spaced in the resting depth of each isopycnal. Lower three rows: same for stations N2b, S6a, and S6b, respectively.

at which internal waves travel as they propagate upward or downward from their sources). The slope depends on stratification and frequency, which is why the curves have greater slope at greater depth. Likewise, the semidiurnal motions (Figure 3, right) have greater slopes than their diurnal counterparts (Figure 3, left). The spacing between the two ridges is significantly greater at the northern line, such that semidiurnal characteristics emanating from the eastern ridge top impinge on the western ridge. At the southern line, the spacing is smaller, making resonance less possible as the characteristics “miss” the western ridge. Although semidiurnal internal wave resonance appears likely in the northern strait, more measurements and modeling are required for certainty.

The horizontal transport or flux of

baroclinic energy assists in identification of radiation from the two ridges and their interference with one another. It is calculated from the correlation between baroclinic velocity u and baroclinic pressure p (i.e., $\langle up \rangle$), with the pressure determined from the density profiles under the hydrostatic assumption. Consider a location between two laterally offset meridional line sources on an east-west line, each giving rise to waves of equal amplitude propagating eastward and westward. Energy between the sources would be expected, but no net east-west energy flux. However, rotation gives rise to alternating bands of meridional (transverse) flux (Nash et al., 2004; Alford and Zhao, 2007; Martini et al., 2010). Just this pattern is seen at the northern section of the ridge, which is demonstrated in the upper

panels of Figure 3 by plotting profiles of energy flux (dark gray) and energy (light gray) at each station. Semidiurnal and diurnal signals are shown at left and right, respectively.

Net flux at station MPN, between the ridges, is nearly zero, consistent with nearly equal but opposite fluxes from the ridges on either side. However, energy flux at the southern line (bottom) is greater and more continuous, indicating that a lesser role is played by the western ridge on that line. This role can be quantified, following Alford and Zhao (2007), by noting that the ratio of the flux to the energy should equal the group velocity c_g for a free wave (e.g., Lighthill, 1978) but be nearly zero for a superposition of waves. West of the western ridge, energy flux is strongly westward, exceeding 60 kW m^{-1} at spring tide,

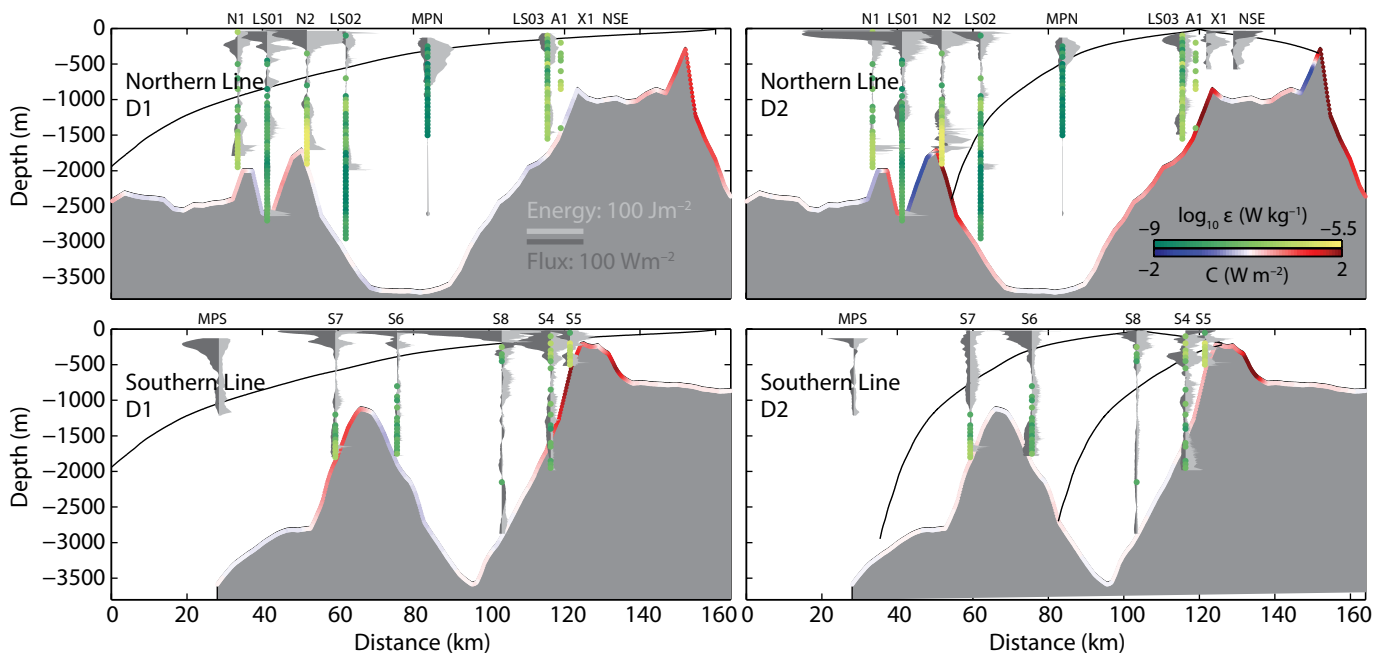


Figure 3. Bathymetry and measured energy flux (dark gray), energy (light gray), and dissipation (colors) for each constituent along each line. Cross sections of model bathymetry (gray shading) and conversion (red/blue) are plotted along the northern line (top panels) and the southern line (bottom), plotted versus distance from the western end of each line (see Figure 1). Left and right panels are for diurnal and semidiurnal components, respectively. Characteristics (see text) computed from the measured stratification are indicated in each panel. At each station, along-line synoptic energy flux profiles are plotted in dark gray, with energy plotted as lighter gray, increasing to the right. Reference bars are given in the upper left panel. Time-mean dissipation rate for each station is plotted in green/yellow at each location (color scale at upper right). Conversion is provided courtesy of Harper Simmons, University of Alaska.

one of the strongest energy flux values observed anywhere in the world ocean. This energy flux is concentrated in the density-stratified water within the upper 500 m and corresponds to the internal tide that is radiated into the deep basin of the South China Sea.

To summarize the results of these recent measurements in Luzon Strait, intense tidal interaction with topography leads to a variety of responses. At the northern end of the strait, where the ridge spacing is close to one internal semidiurnal wavelength, there is evidence of a standing internal wave between the ridges. The observations reveal little net energy flux measured in the center of the strait. The deeper western ridge at the northern line allows enhanced westward radiation of semidiurnal internal tidal energy, but there is only modest radiation of diurnal energy. In contrast, along the southern line, the ridge spacing is less and does not match the semidiurnal wavelength, but there is strong radiation of the diurnal signal, with most of the energy trapped in the upper 500 m.

TIDAL EVOLUTION FROM LUZON STRAIT INTO THE SOUTH CHINA SEA BASIN

To first order and in particular for the first internal mode, conditions for internal tide generation appear consistent with those predicted for the mixed tidal lee wave type (Vlasenko et al., 2005). Although internal hydraulic processes may occur at discrete locations, such as in the northern part of the Heng-Chun Ridge and in a shallower feature south of Sabtang Island (Warn-Varnas et al., 2010), the present evidence points toward predominantly subcritical flow over the ridges (i.e., flow

speed is less than the first mode internal wave speed). Zhang et al.'s (2011) calculations, and their analysis using a simplified model of the first internal mode response, support the notion that internal hydraulic and also lee wave contributions are likely to be weak. Local topography may favor higher modes, but further observations are required to resolve this response. This interpretation is also consistent with the absence of well-defined surface manifestations of nonlinear internal waves in remote sensing imagery within Luzon Strait.

The large internal tides radiating westward from the strait into the deep basin of the South China Sea evolve in a way that depends upon the competing influences of rotational dispersion and nonlinear steepening. For the internal diurnal tide, rotational effects dominate, and steepening is inhibited. Internal semidiurnal tides also respond to rotational effects, but in this case, the steepening proceeds until nonhydrostatic effects become important.

Internal tides radiating into the South China Sea from Luzon Strait are long (~ 135 km for M_2) relative to the vertical scale of stratification (~ 500 m) or the water depth (2–3 km), and do not immediately produce a pronounced surface manifestation sufficient to generate the sharply defined lines seen in remotely sensed images (Figure 1). Signatures of this kind, so clearly identified both in synthetic aperture radar and visible wavelength imagery, depend upon modulation of surface waves by strong surface current divergence produced by short, steep internal waves. Such waves are the result of nonlinear transformation of the internal tide and have been the subject of extensive modeling and theoretical analysis. That these surface

signatures in the South China Sea are consistent with this interpretation has been amply demonstrated by observations. Short-period nonlinear internal waves always occur as the internal tide interacts with the continental slope of mainland China, but their occurrence in the deep basin depends on the character of the tidal forcing.

Remotely sensed wave positions collected by Jackson (2009) over nearly four years show that they first become apparent at $\sim 120.5^\circ\text{E}$, with more frequent occurrences west of 120.0°E . Initially, the remotely sensed waves extend in a north-south arc spanning 100–200 km centered at $\sim 20.5^\circ\text{N}$. Their orientation implies propagation to the west or west-northwest. The position of a remotely sensed wave depends on the time of the satellite overpass, but the distribution of observed wave positions provides support for the conclusion that short nonlinear waves form about 180 km west of the prominent Lan-Yu Ridge and slightly west of the Heng-Chun Ridge. As they approach the continental shelf, they slow down and are refracted, presenting a more complicated picture, with further generation and reflection of the internal tide by the local topography (Klymak et al., 2011).

The steepening of an internal tide and subsequent generation of a train of short nonlinear internal waves has been widely observed in coastal environments. However, Earth's rotation influences this process, and in the South China Sea the waves take approximately one inertial period (33 h at this latitude) to cross the deep basin, providing sufficient time for rotation to influence their evolution.

Observations of the waves at three locations (Figure 1) in Luzon Strait and the deep basin to the west were

acquired over seven months using pressure-sensor equipped inverted echosounders (PIES). Placed on the seafloor, these instruments transmit an acoustic pulse to the sea surface and detect the time it takes for the echo to return. Changes in stratification due to passage of an internal wave produce corresponding changes in acoustic travel time. Background temperature/salinity profiles acquired during the study, together with simultaneous pressure measurements to correct for changes in sea surface elevation, allow inversion to recover time-series measurements of fluctuations in stratification. Such measurements have been widely used to study mesoscale ocean processes. By adapting the instrument to sample rapidly (every 6 s), it is possible to measure the shape of a passing internal wave. Following a pilot study in 2005, analysis of internal waves measured with colocated inverted echosounders and recording thermistor strings showed consistent results (Li et al., 2009). The inverted echosounder measurement is restricted to the first internal mode, as all modes but the first are effectively

removed in the vertical integration. Removal of the higher modes has the benefit of allowing the first mode to be clearly revealed in a way that would not be possible if higher modes were also present. Higher-mode waves undoubtedly exist in the South China Sea and are of interest, but they are usually left behind by the fast-moving first mode response and are generally less energetic. By tracking waves as they pass successive instruments, we can observe the progressive evolution of the internal tide from its initial formation in Luzon Strait to its subsequent transformation under the influence of nonlinearity and rotation.

The tidal currents in Luzon Strait change between predominantly diurnal and predominantly semidiurnal, separated by a transition period of mixed tides. This change is illustrated in Figure 4 (upper panel) where the predicted tidal current is separated into diurnal (red) and semidiurnal (blue), based on the four leading constituents in each case. Figure 4 (lower panel) shows the occurrence and amplitude of the short-period nonlinear internal waves observed at station A3 in the deep

basin, based on high-pass filtering of the PIES time series; only the leading wave of a wave packet is shown. Comparison with the predicted tidal currents shows a tendency for short-period nonlinear internal waves in the deep basin to coincide with maxima in the semidiurnal tidal current rather than the diurnal current, even though the latter can be stronger than the semidiurnal signal. There is also a tendency for the strongest internal solitons to occur when the diurnal and semidiurnal currents are in phase.

Theoretical models provide insight into the combined effects of nonlinearity and rotation. In the South China Sea, a useful simplification, consistent with the limitation of our measurements to the first internal mode, represents stratification as a two-layer system with a warm surface layer overlying a deeper cold layer. Nonlinearity distorts the wave as it travels. For example, in the absence of rotation, a sinusoidal internal tide generated by harmonic forcing initially evolves toward a saw-tooth shape as an interface with positive slope progressively steepens and

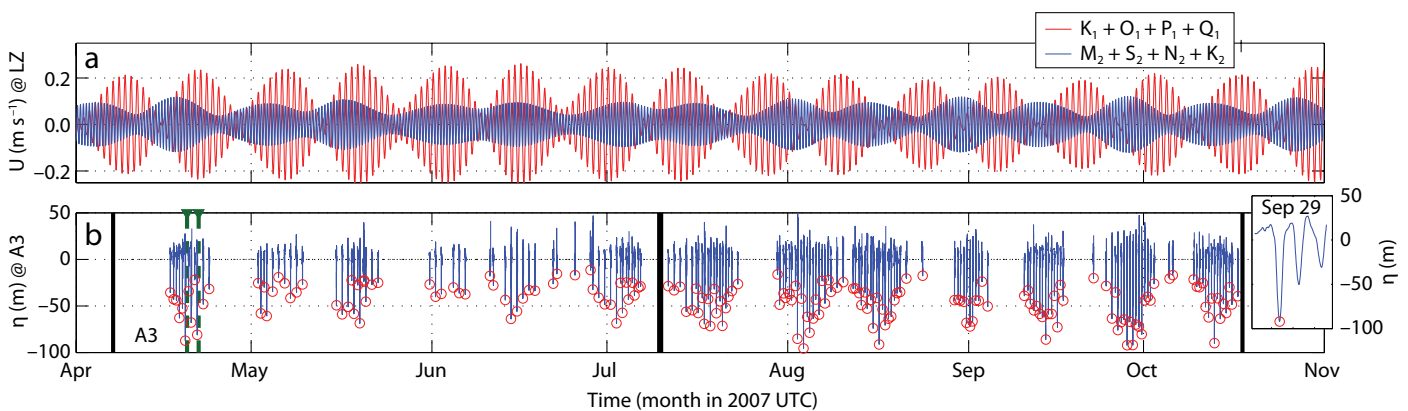


Figure 4. Upper panel: Tidal current predictions (TPXO) for Luzon Strait broken into diurnal (red) and semidiurnal (blue) components, each based on the four leading constituents. Lower panel: Occurrence and range of nonlinear waves derived from high-pass filtered PIES time series. Only the leading wave of a wave train is shown. Nonlinear internal waves tend to occur when the semidiurnal tidal current envelope in Luzon Strait is at its maximum. Dashed lines indicate the period of observations shown in Figure 6. Adapted from Li and Farmer, 2011

an interface of negative slope becomes less steep. The greater the amplitude of the initial wave, the more rapidly the nonlinear transformation occurs. When the interfacial slope becomes sufficiently steep, vertical acceleration plays a role (the “nonhydrostatic effect”), and short-period waves are generated. It is these short nonlinear waves of large amplitude that are responsible for the surface signatures seen so clearly in remotely sensed images (Figure 1).

Earth’s rotation plays a different role. As the interface steepens, the flow is deflected to the right in the Northern Hemisphere, dispersing energy from the internal tide into internal inertial waves, thus tending to inhibit further steepening. The rotational effect for semidiurnal tides in the South China Sea is small enough that steepening is diminished but not halted, continuing until vertical acceleration becomes important and short-period internal solitary waves are generated. For diurnal internal tides, which have a period closer to the inertial period, rotation inhibits steepening and the internal tide assumes a cusp shape, with the downward-pointing cusp identified as a “corner wave.” This interpretation helps explain the increased tendency for nonlinear internal waves to be more closely associated with semidiurnal rather than diurnal currents, although, as noted above, nonlinear internal waves always form further west as they slow down over the continental slope. Modeling (Helfrich, 2007) shows that these shape changes are not permanent features; over a long enough time period, the inertial energy would be returned to the internal tide and the process of steepening and rotational dispersion repeated. In the South China Sea, however, interaction with the continental shelf occurs

long before that could happen.

A useful scaling parameter, referred to as the Ostrovsky number O_s , is found from the ratio of nonlinear to rotational terms in the weakly nonlinear two-layer case:

$$O_s = 36\pi^2 Ag'(|h_1 - h_2| / h_1 + h_2) / f^2\lambda^2, \quad (1)$$

where A is the internal wave amplitude, $g' = g \Delta\rho/\bar{\rho}$ is the reduced gravity ($\Delta\rho/\bar{\rho}$ is the relative density difference between layers), λ is the wavelength, and h_1 and h_2 are the upper and lower layer depths, respectively. For $O_s \gg 1$, the waves steepen and “break,” whereas for $O_s \ll 1$, no breaking occurs. For $1 < O_s < \sim 2$, rotation inhibits steepening, the steepest part of the interface shifts forward, and the internal tide approximates a parabolic or “corner wave” as predicted by Ostrovsky (1978) and explored in

depth by Helfrich (2007). This simplified description applies to a single tidal component. The more realistic combination of diurnal and semidiurnal internal tides leads to a more subtle interaction and Equation 1 no longer strictly applies, although we can use an approximation \tilde{O}_s based on the initial (positive) interface slope (Farmer et al., 2009). Moreover, the waves in the South China Sea are large and can be steep, justifying a fully nonlinear analysis.

Figure 5 illustrates results of an analysis by Li and Farmer (2011), based on Hibiyā’s (1986) solution for internal tide generation. The resulting internal tide provides initial conditions for analysis of the nonlinear evolution using Helfrich’s (2007) fully nonlinear wave evolution model. Meridionally averaged topography, including both

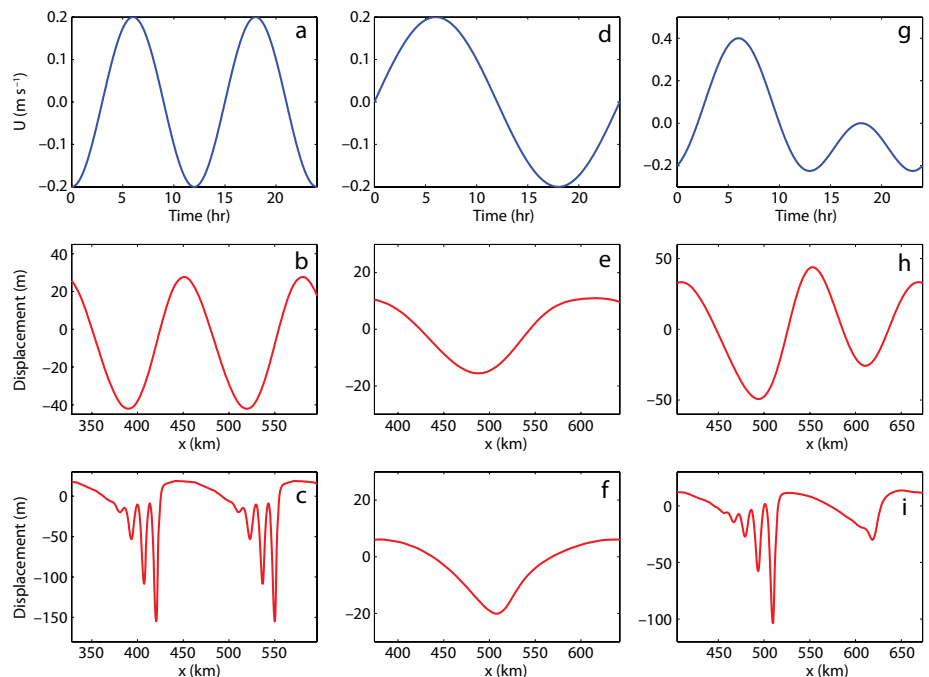


Figure 5. Two-layer model solutions for internal tides generated in Luzon Strait. Top row: Three representative tidal current conditions in Luzon Strait corresponding to (a) predominantly semi-diurnal, (d) predominantly diurnal, and (g) mixed forcing. Middle row: Interface displacement solutions to Hibiyā’s (1986) internal tide generation model for a two-ridge system representative of the strait at 21°N, evaluated for each example in the top row. Bottom row: Evolution of internal tide for each internal tide shown in the middle row, calculated for station A3 using Helfrich’s (2007) fully nonlinear model. Adapted from Li and Farmer, 2011

ridges between 20°N and 21°N, is included in the internal tide generation, with a ridge spacing matching the semidiurnal wavelength. The calculations are for three idealized but representative tidal current conditions in Luzon Strait: a purely semidiurnal tide (a, b, c), a diurnal tide (d, e, f), and

a characteristic feature also observed in the South China Sea.

Figure 6 shows a short section of the PIES time series during a period of mixed tidal forcing, referenced in Figure 4, illustrating the alternating character of the response predicted for the idealized case (g, h, i) shown above. The

2006; Alford et al., 2010). To the east of Dongsha Plateau, these westward-propagating nonlinear internal waves slow down and become unstable as they encounter a steep slope, from ~ 2,500 m depth east of 118°E to ~ 300 m on the Dongsha Plateau at 117°E, forming recirculating cores, with individual waves sometimes being scattered into multiple waves and even becoming inverted.

In 2005, a Nonlinear Internal Wave Initiative pilot study tracked the evolution of shoaling nonlinear internal waves on the steep slope between 117.5°E and 117°E (yellow box in Figure 1) with shipboard profiling of currents, salinity, and temperature (ADCP and CTD), using the Taiwanese research vessel *Ocean Researcher 3*. Figure 7

shows an example of a large-amplitude nonlinear internal wave measured by a rapidly profiling CTD at 21°N, 117.25°E, acquired in water of 440 m depth. Based on 10 CTD profiles, the isopycnal surface of 1,024 kg m⁻³ descends from 50 m depth before the arrival of the nonlinear internal wave to 200 m depth at the center of the wave, a vertical excursion of ~ 150 m. The wave has a width of ~ 1 km. Within the wave, a gravitationally unstable overturn exists between ~ 100 m and 175 m depth. In sharp contrast to the gradual steepening process and generation of short-period nonlinear internal waves described

“ LUZON STRAIT AND THE SOUTH CHINA SEA PROVIDE AN IDEAL LABORATORY FOR STUDYING THE GENERATION, EVOLUTION, AND ULTIMATE FATE OF LARGE-AMPLITUDE INTERNAL WAVES. ”

a mixed tide (g, h, i). The top row shows the prescribed zonal current in Luzon Strait for each case, with the second row showing the corresponding internal tide that is generated, and the bottom row giving the modeled nonlinearly evolved wave after it has travelled 30 h, which is the approximate distance to station A3 (Figure 1). For the semidiurnal example, $O_s \sim 2$ and the waves have steepened to form solitary wave packets. For the diurnal case $O_s \sim 1$, the internal tide has evolved into a “corner wave.” For the mixed example, \tilde{O}_s alternates between ~ 1 and ~ 2, leading to an alternating pattern of single and multiple waves,

internal tides that traverse the deep basin of the South China Sea are progressively transformed by nonlinearity and rotation in this way, until they approach the continental shelf where the changing depth becomes the dominant factor in their further evolution.

INTERACTION OF NONLINEAR INTERNAL WAVES WITH THE DONGSHA PLATEAU

Nonlinear internal waves propagate predominantly westward at a speed of 2–3 m s⁻¹ across the deep South China Sea basin without losing much of their energy and identity (Klymak et al.,

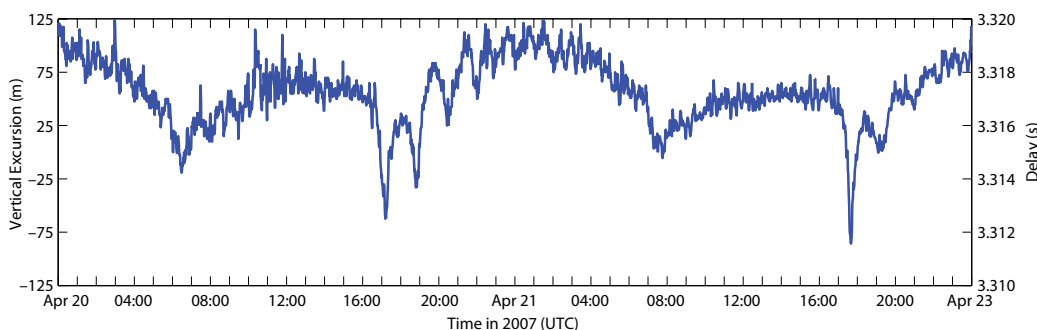


Figure 6. Example time series of PIES acoustic travel time at station A3 during mixed tidal currents. The measurement period is shown by vertical dashed lines in the lower panel of Figure 4. The travel time (right-hand scale) has been converted to displacement of vertical stratification (left-hand scale) based on a first internal mode analysis.

above, this wave exhibits an extreme breaking process and has formed a recirculating trapped core in the center of the wave. Breaking of internal waves, defined as occurring when the particle velocity (current associated with the wave) exceeds the wave's propagation speed (Lamb, 2002), is a specific feature of these observations. Moreover, the ADCP measurements show closed streamline flow, and repeated CTD profiles reveal overturning of the density stratification. This is the internal wave analog of breaking surface waves when they shoal near the beach and the crest advances faster than the trough, but with an amplitude 10–100 times greater. Echosounder images proved effective at tracking the waves as they moved at 1–2 m s⁻¹ across Dongsha Plateau. Waves propagating across the plateau dissipate most of their energy before reaching the continental shelf (Lien et al., 2005; Chang et al., 2006).

The nonlinear internal waves in the South China Sea (Chang et al., 2008) strongly modulate the surface waves. Strong horizontal convergence in the leading portion of the wave often leads to surface-wave breaking on the slope of Dongsha (Figure 8) where strong surface scattering intensity is detected in remotely sensed synthetic aperture radar images and shipboard radar. Behind the wave, horizontal divergence and boils associated with upwelling are present. Schools of pilot whales are often observed in the boil region. Nonlinear internal waves appear to lead to the aggregation of prey as they entrain small fish and squid within convergence zones. These boils occur near the leading part of the wave, accompanied by downwelling, and at greater depth in the trailing portion of the wave, accompanied by upwelling.

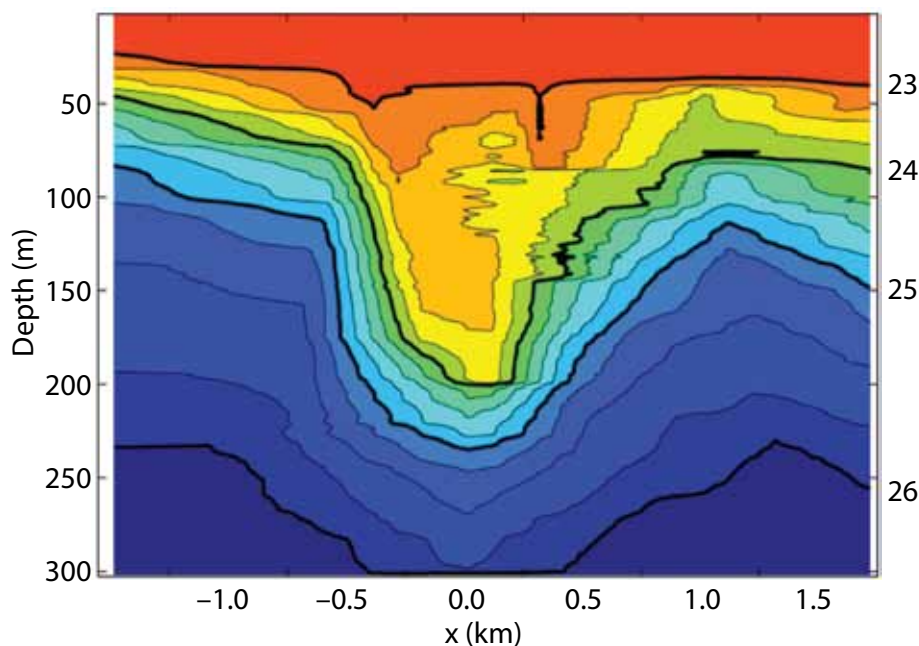


Figure 7. A large-amplitude nonlinear internal wave observed from a shipboard conductivity-temperature-depth survey around 21°N, 117.25°E. Color shadings and contour lines are isopycnals at 0.25 kg m⁻³ interval. Isopycnal surfaces of 1,023, 1,024, 1,025, and 1,026 kg m⁻³ are labeled.

Active movement of the prey likely plays a role in the aggregative process. Prey availability for pilot whales and the marine ecosystem in the South China Sea are likely influenced by the characteristics of nonlinear internal waves, which in turn are modulated by the spring neap tidal cycle (Moore and Lien, 2007).

OUTSTANDING PROBLEMS

While the broad concepts of generation, evolution, and dissipation of these remarkable and widely distributed waves are apparent, there are many subtleties yet to be resolved, including:

The role of the Kuroshio in modulating internal wave generation. Model calculations (Buijsman, 2010b) predict how westward shoaling of stratification associated with the Kuroshio enhances the amplitude and nonlinearity of internal tides traveling into the South China Sea relative to those traveling into the Pacific.

If there is an intrusion of the Kuroshio into the South China Sea, an additional effect comes into play due to Doppler shifting of the radiated internal tides by the zonal component of the background current (Li and Farmer, 2011). These predictions need to be tested against observations over periods long enough to include variability in the Kuroshio together with time series measurements east of the eastern ridge to observe waves radiating into the Pacific.

Detailed understanding of wave generation, including generation of intense turbulence over ridges, generation of higher-mode components, nonlinear interaction of waves in Luzon Strait, and related phenomena.

The pioneering observations in Luzon Strait described above could not resolve some important details of the generation process. Are there locations of hydraulically controlled flow, and if so, how important are these flows to the far-field

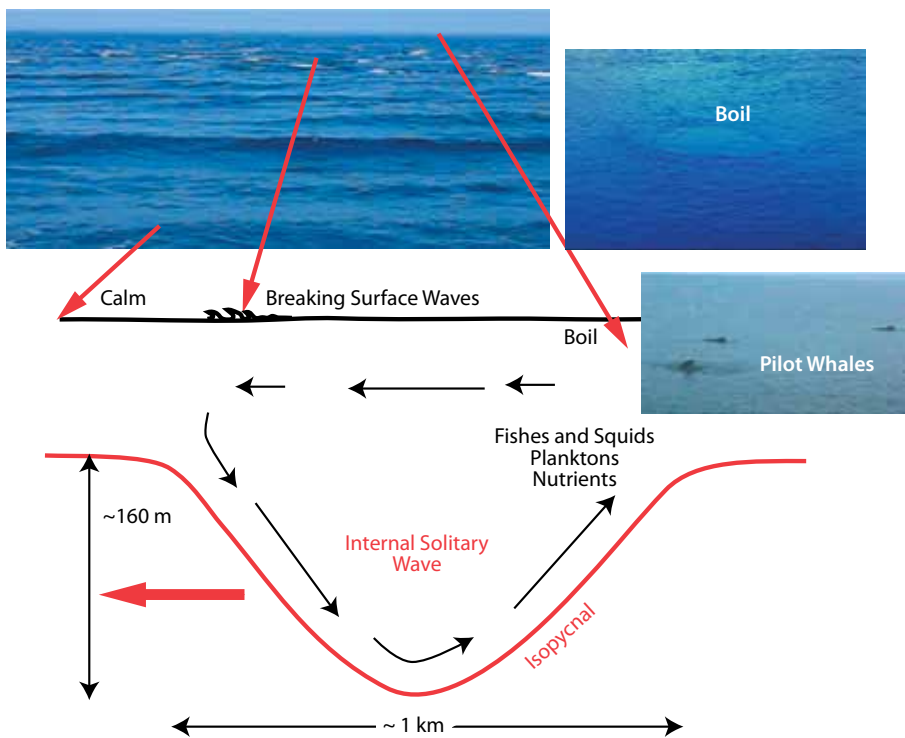


Figure 8. Snapshots of varying sea-surface conditions associated with internal waves coupled to a schematic diagram showing the associated spatial scale. Arrow sequence indicates current pattern associated with overturning of the wave core. Strong horizontal convergence and vertical downwelling in the front portion of the internal wave leads to breaking surface waves; horizontal divergence and upwelling in the rear portion of the wave, where pilot whales were seen, create surface boils and may entrain fish, squid, plankton, and nutrients, and thus the pilot whales.

internal wave properties? Are lee waves generated in some areas, and how do they evolve? What fraction of energy goes into higher modes? What role do these higher modes play in contributing to turbulence, mixing, and far-field internal wave characteristics?

The far-field consequences of predominant diurnal internal tide radiation from the southern portion of the strait (see Figure 3) and how wave generation at different frequencies (diurnal and semidiurnal) at different locations combines to form the observed features in the deep basin. Diurnal and semidiurnal internal tides respond quite differently to the combined effects of nonlinearity and rotation. Further observations and

model calculations are required to understand how spatial variations among different components interact to form the far-field signal.


Tidal interaction with Dongsha Plateau and the continental slope, which not only intensifies and dissipates internal waves that have propagated across the deep basin from the east but also is a source of additional internal tide generation, turbulence, and mixing. Observations show a complex pattern of nonlinear internal waves over the shelf and shelf break. Interesting effects can be expected due to the interaction of waves propagating in different directions.

How to use described biological effects of the internal waves to make quantitative estimates of the role these waves play in biological productivity in the South China Sea.

Vertical mixing associated with the internal waves brings nutrients into the euphotic zone. The extent to which this fertilization of near-surface waters occurs in the South China Sea and the resulting biological impact represent a potentially important feature of this highly productive part of the ocean.

Luzon Strait and the South China Sea provide an ideal laboratory for studying the generation, evolution, and ultimate fate of large-amplitude internal waves. While the observations and analyses of recent studies have greatly improved our understanding, much remains to be learned about these energetic and oceanographically significant phenomena.

ACKNOWLEDGEMENTS

The work described here owes much to the encouragement and support of the US Office of Naval Research Physical Oceanography Program's Nonlinear Internal Waves Initiative and Internal Waves in Straits Experiment, which have in turn benefitted greatly from the US-Taiwanese collaboration, including important Taiwanese scientific and logistical support. We thank the captains and crews of all the US and Taiwanese research vessels conducting this research, as well as the technical staffs of each institution, for their skill and expertise—without which the fieldwork would not have been possible. We also thank the many colleagues and technical support staff who have played important roles in ensuring the success of our research. 

REFERENCES

- Alford, A., and Z. Zhao. 2007. Global patterns of low-mode internal-wave propagation. Part II. Group velocity. *Journal of Physical Oceanography* 33:1,510–1,527, <http://dx.doi.org/10.1175/JPO3086.1>.
- Alford, M.H., M.C. Gregg, and M.A. Merrifield. 2006. Structure, propagation and mixing of energetic baroclinic tides in Mamala Bay, Oahu, Hawaii. *Journal of Physical Oceanography* 36:997–1,018, <http://dx.doi.org/10.1175/JPO2877.1>.
- Alford, M.H., R.-C. Lien, H. Simmons, J. Klymak, S. Ramp, Y.J. Yang, D. Tang, and M.-H. Chang. 2010. Speed and evolution of nonlinear internal waves transiting the South China Sea. *Journal of Physical Oceanography* 40:1,338–1,355, <http://dx.doi.org/10.1175/2010JPO4388.1>.
- Alford, M.H., J.A. MacKinnon, J.D. Nash, H. Simmons, A. Pickering, J.M. Klymak, R. Pinkel, O. Sun, L. Rainville, R. Musgrave, and others. 2011. Energy flux and dissipation in Luzon Strait: Two tales of two ridges. *Journal of Physical Oceanography*, <http://dx.doi.org/10.1175/JPO-D-11-073.1>.
- Buijsman, M.C., Y. Kanarska, and J.C. McWilliams. 2010a. On the generation and evolution of nonlinear internal waves in the South China Sea. *Journal of Geophysical Research* 115, C02012, <http://dx.doi.org/10.1029/2009JC005275>.
- Buijsman, M.C., J.C. McWilliams, and C.R. Jackson. 2010b. East-west asymmetry in nonlinear internal waves from Luzon Strait. *Journal of Geophysical Research* 115, C10057, <http://dx.doi.org/10.1029/2009JC006004>.
- Chang, M.-H., R.-C. Lien, T.Y. Tang, E.A. D'Asaro, and Y.J. Yang. 2006. Energy flux of nonlinear internal waves in northern South China Sea. *Geophysical Research Letters* 33, L03607, <http://dx.doi.org/10.1029/2005GL025196>.
- Chang, M.-H., R.-C. Lien, T.Y. Tang, Y.J. Yang, and J. Wang. 2008. A composite view of surface signatures and interior properties of nonlinear internal waves: Observations and applications. *Journal of Atmospheric and Oceanic Technology* 25:1,218–1,227, <http://dx.doi.org/10.1175/2007JTECHO574.1>.
- Dillon, T.M. 1982. Vertical overturns: A comparison of Thorpe and Ozmidov length scales. *Journal of Geophysical Research* 87:9,601–9,613, <http://dx.doi.org/10.1029/JC087iC12p09601>.
- Echeverri, P., and T. Peacock. 2010. Internal tide generation by arbitrary two-dimensional topography. *Journal of Fluid Mechanics* 659:247–266.
- Farmer, D.M., Q. Li, and J.-H. Park. 2009. Internal wave observations in the South China Sea: The role of rotation and nonlinearity. *Atmosphere-Ocean* 47:267–280, <http://dx.doi.org/10.3137/OC313.2009>.
- Gregg, M. 1989. Scaling turbulent dissipation in the thermocline. *Journal of Geophysical Research* 94:9,686–9,698, <http://dx.doi.org/10.1029/JC094iC07p09686>.
- Helfrich, K.R. 2007. Decay and return of internal solitary waves with rotation. *Physics of Fluids* 19, 026601, <http://dx.doi.org/10.1063/1.2472509>.
- Hibiya, T. 1986. Generation mechanism of internal waves by tidal flow over a sill. *Journal of Geophysical Research* 91:7,697–7,708.
- Jackson, C.R. 2009. An empirical model for estimating the geographic location of nonlinear internal solitary waves. *Journal of Atmospheric and Oceanic Technology* 26:2,243–2,255, <http://dx.doi.org/10.1175/2009JTECHO638.1>.
- Klymak, J.M., M.H. Alford, R. Pinkel, R.-C. Lien, Y.J. Yang, and T.-Y. Tang. 2011. The breaking and scattering of the internal tide on a continental slope. *Journal of Physical Oceanography* 41:926–945, <http://dx.doi.org/10.1175/2010JPO4500.1>.
- Klymak, J.M., R. Pinkel, C.-T. Liu, A.K. Liu, and L. David. 2006. Prototypical solitons in the South China Sea. *Journal of Geophysical Research* 33, L11607, <http://dx.doi.org/10.1029/2006GL025932>.
- Lamb, K.G. 2002. A numerical investigation of solitary internal waves with trapped cores formed via shoaling. *Journal of Fluid Mechanics* 451:109–144, <http://dx.doi.org/10.1017/S002211200100636X>.
- Li, Q., and D.M. Farmer. 2011. The generation and evolution of nonlinear internal waves in the deep basin of the South China Sea. *Journal of Physical Oceanography* 41:1,345–1,363, <http://dx.doi.org/10.1175/2011JPO4587.1>.
- Li, Q., D.M. Farmer, T.F. Duda, and S. Ramp. 2009. Acoustical measurement of nonlinear internal waves using the inverted echo sounder. *Journal of Atmospheric and Oceanic Technology* 26:2,228–2,242, <http://dx.doi.org/10.1175/2009JTECHO652.1>.
- Lien, R.-C., T.Y. Tang, M.H. Chang, and E.A. D'Asaro. 2005. Energy of nonlinear internal waves in the South China Sea. *Geophysical Research Letters* 32, L05615, <http://dx.doi.org/10.1029/2004GL022012>.
- Lighthill, J. 1978. *Waves in Fluids*. Cambridge University Press, New York, 524 pp.
- Martini, K.I., M.H. Alford, E. Kunze, S.M. Kelly, and J.D. Nash. 2011. Observations of internal tides on the Oregon continental slope. *Journal of Physical Oceanography* 41:1,772–1,794, <http://dx.doi.org/10.1175/2011JPO4581.1>.
- Moore, S.E., and R.-C. Lien. 2007. Pilot whales follow internal solitary waves in the South China Sea. *Marine Mammal Science* 23:193–196, <http://dx.doi.org/10.1111/j.1748-7692.2006.00086.x>.
- Munk, W. 1966. Abyssal recipes. *Deep Sea Research and Oceanographic Abstracts* 13:707–730.
- Nash, J.D., E. Kunze, J.M. Toole, and R.W. Schmitt. 2004. Internal tide reflection and turbulent mixing on the continental slope. *Journal of Physical Oceanography* 34:1,117–1,134, [http://dx.doi.org/10.1175/1520-0485\(2004\)034<1117:ITRATM>2.0.CO;2](http://dx.doi.org/10.1175/1520-0485(2004)034<1117:ITRATM>2.0.CO;2).
- Ostrovsky, V.A. 1978. Nonlinear internal waves in a rotating ocean. *Oceanology* 18:119–125.
- Rudnick, D., S. Jan, L. Centurioni, C.M. Lee, R.-C. Lien, J. Wang, D.-K. Lee, R.-S. Tseng, Y.Y. Kim, and C.-S. Chern. 2011. Seasonal and mesoscale variability of the Kuroshio near its origin. *Oceanography* 24(4):52–63, <http://dx.doi.org/10.5670/oceanog.2011.95>.
- Thorpe, S.A. 1977. Turbulence and mixing in a Scottish Loch. *Philosophical Transactions of the Royal Society of London. Series A, Mathematical and Physical Sciences* 286(1334):125–181.
- Vlasenko, V., N. Stashchuk, and K. Hutter. 2005. *Baroclinic Tides: Theoretical Modeling and Observational Evidence*. Cambridge University Press, 351 pp.
- Warn-Varnas, A., J. Hawkins, K.G. Lamb, S. Piacsek, S. Chin-Bing, D. King, and G. Burgos. 2010. Solitary wave generation dynamics in Luzon Strait. *Ocean Modelling* 31:9–27, <http://dx.doi.org/10.1016/j.ocemod.2009.08.002>.
- Zhang, Z., O.B. Fringer, and S.R. Ramp. 2011. Three-dimensional, nonhydrostatic numerical simulation of nonlinear internal wave generation and propagation in the South China Sea. *Journal of Geophysical Research* 116, C05022, <http://dx.doi.org/10.1029/2010JC006424>.